

High Frequency Performance of GaN Based IMPATT Diodes

B. Chakrabarti

Department of ECE, Bengal Institute of Technology, Kolkata-150, India

chakrabortybibek@yahoo.co.in

D. Ghosh

Department of ECE, Swami Vivekananda Institute of Science and Technology, Kolkata-145

India dg1036@yahoo.com

M. Mitra

Dept. of E&TC Engg., BESU, Shibpur, Howrah 711103, W.B., India

monojit_m1@yahoo.co.in

Abstract:

IMPATT is a p^+n junction diode reversed bias to breakdown and can generate microwave power when properly embedded in a resonant cavity. Till emergence on 1965 day by day it became more powerful solid state source for microwave as well as mm-wave frequency range. To get higher efficiency and power output different structures like SDR, DDR, DAR, lo-high-lo, etc. were proposed and developed by different scientists over the years. Then the IMPATT development started with different semiconductor materials like GaAs, InP, GaN, etc. along with Silicon to achieve higher efficiency, power output and frequency range. In this paper the performance of GaN based SDR IMPATT have thoroughly studied in terms of (i) electric field profile $[E(x)]$ (ii) normalized current density profile $[P(x)]$ (iii) Susceptance Vs Conductance characteristics (iv) RF power output (v) negative resistivity profile $[R(x)]$ of the diodes through simulation scheme. It is being observed that the efficiency is 17.9% at Ka-band and because of the very high breakdown voltage, power output is as high as 1.56W in comparison with other frequency band of operations.

Key words: mm wave IMPATT, GaN IMPATT, Ka-band IMPATT oscillator, simulation of IMPATT

1. Introduction:

Over the years it is being found that IMPact Avalanche Transit Time (IMPATT) diodes became most powerful solid state sources in the mm-wave and sub-mm wave frequencies. These devices are now used as transmitter in radars, as a source in the missile seeker head and in many others mm-wave civilian and military applications [Trew et. al. 2005], which includes communication.

Low atmospheric attenuation and high penetrating power of mm-wave signals through cloud, dust and fog at window frequencies have made millimeter wave communication systems very attractive. 36GHz (Ka-band), 60 GHz (V-band), 94 GHz (w-band) are such atmospheric window frequencies around which large research activities in the field of mm-wave communication are going on. During initial phases of development of IMPATT devices GaAs (Gallium Arsenide) and Si (Silicon) were mainly used as substrate semiconductor materials for IMPATT fabrication. But because of the limited power and operating frequencies of Silicon and GaAs IMPATTs, development started with the fabrication of IMPATT devices based on wide band gap (WBG) semiconductors like Silicon Carbide (SiC) and Gallium Nitride (GaN). These materials can withstand high value of critical electric field (E_c) and having high carrier saturation velocity (V_s), and at the same time having high thermal conductivity (K). The critical electric field for dielectric breakdown and the thermal conductivity of the material determines the maximum power handling capability of the device. The breakdown field (E_c) places a fundamental limitation on the RF power that can be converted from the dc bias and thermal conductivity (K) determines the ease with which the unconverted dc power can be extracted from the device. The dielectric constant (ϵ) and band gap (E_g) are also important material parameters for the analysis, because the

dielectric constant determines the device impedance and band gap determines the upper temperature limit for the safe operation of the device. As it can be seen from the Table: 1 that wide band gap semiconductor material such as GaN have (i) seven times higher E_c and (ii) two times higher V_s in comparison to those of Si and GaAs. Also review works on wide band gap semiconductor establishes the superiority of GaN based high power and high frequency devices [Okumura et. al., 2006]. Overall it is found that high quality GaN films can be grown easily on SiC substrates by MOCVD [Inoki et. al.2003].

The two common types of GaN are, Wurtzite and Zinc-blend .Wurtzite phase (Wz) GaN based IMPATTs have found to perform better than Zinc-blend (ZnB) GaN, in terms of breakdown voltage, efficiency and power output at around 140 GHz [Panda et. al. 2001]. At the same time detail analysis on the dc and small signal properties of GaN (Wz) based IMPATT diodes and there comparative studies have not been reported so far in recent literatures. The authors have taken SDR ($p^+n^+n^+$) (fig:1) structure of GaN IMPATT diode to simulate the dc and small signal behaviors for optimized operation at different mm-wave window frequency bands. The device dimensions, doping and current densities of the diodes (Wz-GaN) are also optimized for Ka, V and W band frequencies after a detailed computer analysis. Then for a known area of the diode and negative conductance, using the procedure described in literature [Eisele et. al. 1997] the RF power generated from the device was simulated.

The analysis of this paper will be extremely helpful for the design of high power, high frequency GaN (Wz) based IMPATT diodes.

2. Material parameters and simulation method:

For the present analysis, a flat profile SDR (n^+np^+) structure is considered (figure:1), where n^+ and p^+ are highly doped substrates and top layer respectively, and n is the epi-layer. Experimental values of carrier ionization rates [Electronic Archieve, 2011], Monte Carlo simulated temperature dependent ($300k < T < 600k$) values of drift velocity and mobility of charge carriers in hexagonal (Wz) GaN are considered for the simulation work [Mukherjee et. al, 2007 & Kunihiro et. al. 1999]. All the material parameters values which have been considered for simulation are summarized in table1.

Table 1: Comparison of material parameters of GaN polytypes with Si and GaAs (at 300k)

Material & physical properties	Wz-GaN	Znb-GaN	Si	GaAs
Band gap(eV) (E_g)	3.45	3.28	1.12	1.43
Relative dielectric constant(ϵ_r)	8.9	9.7	11.9	13.1
Electric breakdown field E_c (10^7 $v m^{-1}$)	20	20	3	4
Saturated electron drift velocity (10^5 ms^{-1})	2.5	2.0	1	1.2
Electron mobility μ_n ($m^2 v^{-1} s^{-1}$)	0.125	0.10	0.15	0.85
Thermal conductivity K ($w m^{-1} k^{-1}$)	225	130	1.50	46

2.1 DC Analysis

The static characteristics, such as electric field profile and normalized current density profile of the designed diode are obtained following the D.C method [Mukherjee et. al, 2007]. In the dc method, the numerical computation starts from the field maxima near the metallurgical junction. The distribution of dc electric field and carrier currents in the depletion layer are obtained by a double-iterative simulation method, which involves iteration over the magnitude of field maximum (E_m) and its location in the depletion layer. At each point in the depletion layer simultaneous solutions of Poisson and carrier continuity equations are used. The field boundary conditions are given by,

$$E(-x_1)=0 \quad \text{and} \quad E(+x_2)=0 \quad (1)$$

Here $-x_1$ and x_2 represent the edges of the depletion layer in n^+ and p^+ regions, respectively.

The boundary conditions for normalized current density $P(x)$, are given by,

$$P(-x_1)=(2/M_p - 1) \quad \text{and} \quad P(x_2)=(1 - 2/M_n) \quad (2)$$

where, $M_n = J/J_{ns}$, $M_p = J/J_{ps}$; J_{ns} and J_{ps} are electron and hole leakage current densities, respectively.

M_n and M_p are hole and electron current multiplication factors, respectively.

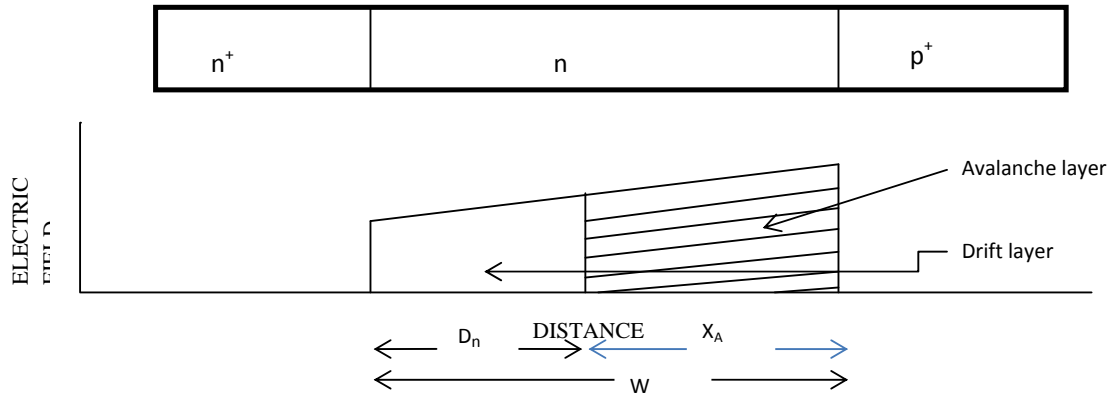


Figure 1. Schematic diode structure and electric field profile. X_A =Width of the Avalanche region, D_n =Width of the Drift region, W =Total depletion layer width

Where $P(x)=(J_p-J_n)/J$, where J_p = hole current density, J_n = electron current density and J total current density.

Thus the dc electric field and current profiles are obtained from simultaneously solution of Poisson and carrier continuity equations, when boundary conditions (1) and (2) are satisfied. The realistic field dependence of electron and hole ionization rates, carrier mobility and the drift velocities of electron and hole are also considered in the simulation program.

The dc to mm-wave conversion efficiency [Sze et. al. 1991] is calculated from the approximate formula,

$$\eta(\%) = (V_D \times 100) / (\pi \times V_B) \quad (3)$$

Where, V_D =voltage drop across the drift region. Also $V_D = V_B - V_A$, where V_A = voltage drop across the avalanche region, and V_B = breakdown voltage.

Avalanche breakdown occurs in the junction when the electric field is large enough such that the charge multiplication factors (M_n, M_p) become very large. The breakdown voltage is calculated by integrating the spatial field profile over the total depletion layer width.

$$V_B = \int_{-x_1}^{+x_2} E(x) dx \quad (4)$$

Where $-x_1$ = n-side depletion layer width

And $+x_2$ = p-side depletion layer width

The results of the dc analysis are then used in the small signal analysis, described briefly in the next sub-section.

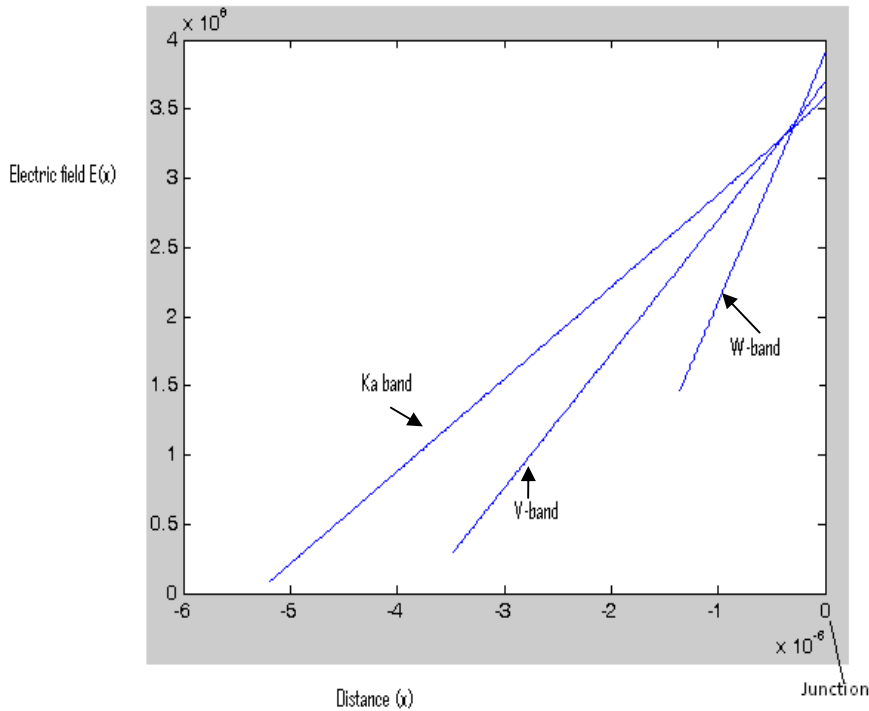


Figure 2: Electric field profiles of SDR n⁺np⁺ IMPATT diode at Ka-band, V-band and W-band respectively.

2.2 Small signal analysis

The Gummel-Blue method [Gummel et. al. 1967] has been followed to compute the negative conductance of the diode at different frequency bands. The dc electric field and current profiles, which are obtained from the D.C analysis, are fed as input data for the small signal analysis. The real part $R(x, \omega)$ and imaginary part $X(x, \omega)$ are obtained by splitting the diode impedance $Z(x, \omega)$ using Gummel-Blue method and thus two different equations are framed [Mukherjee et. al, 2007]. Then, by using modified Runge-Kutta method the solutions of these two equations are found following a double iterative simulation scheme. The small signal parameters like negative conductance(-G), susceptance (B), impedance (Z) of the diode and the range of frequencies over which the diode exhibits negative conductance are found after satisfying the boundary conditions derived elsewhere [Kunihiro et. al. 1999, & Mukherjee et. al, 2010].

The diode negative resistance ($-Z_R$) and reactance ($-Z_x$) are computed through numerical integration of the $-R(x)$ and $-X(x)$ profiles over the active space charge layer. Thus

$$-Z_R = -x_1 \int_{-x_1}^{x_2} -R \, dx \quad \text{and} \quad -Z_x = -x_1 \int_{-x_1}^{x_2} -X \, dx$$

The diode impedance Z is given by,

$$Z(\omega) = -x_1 \int_{-x_1}^{x_2} Z(x, \omega) \, dx = -Z_R + Z_x \tag{5}$$

The diode admittance is expressed as

$$Y = 1/Z = -G + jB = 1/(-Z_R + jZ_x) \tag{6}$$

or, $-G = -Z_R/((Z_R)^2 + (Z_x)^2)$ and $B = Z_x/((Z_R)^2 + (Z_x)^2)$

-G and B are both normalized in accordance with the diode area.

The Avalanche (resonance) frequency (f_a) is a frequency at which the imaginary part, susceptance (B) of the admittance changes its nature from inductive to capacitive. The small signal quality factor (Q_p) is defined as the ratio of the imaginary part of the admittance (at the peak frequency), i.e.

$$-Q_p = (B_p / -G_p) \tag{7}$$

At a given bias current density, the peak frequency (f_p) is the frequency at which the magnitude of the negative conductance of the diode is maximum, and the quality factor is minimum. At f_p , the maximum RF power (P_{RF}) from the device is obtained from the expression [Eisele et. al. 1997]. The area of the diode is considered to be $5 \times 10^{-11} \text{ m}^2$. Under small signal condition V_{RF} (the amplitude of the RF swing) is taken as $V_B/5$ [Majumder et. al. 1997 & 1989].

3. Results and Discussions

The D.C simulation program has been used here to obtain the electric field profile [E(x)] and normalized current density profile [P(x)] of the SDR IMPATT (GaN) diode which is optimized at different mm-wave window frequency bands. The optimized design parameters of the designed diodes are summarized in table: 2

Table2: Design parameters of GaN based SDR IMPATT diodes

Diode Type	Design band	Epilayer doping concentration (n region) (10^{23} m^{-3})	Width of the epilayer(n region)(μm)	Current density(A/m^2)
Flat doping profile	Ka (27-40 GHz)	0.35	5.2	1×10^8
	V (40-60 GHz)	0.5	3.48	1×10^8
	W (75-110 GHz)	0.9	1.25	1×10^8

Table3: D.C and small signal analysis result

Design Band	E_m (10^8vm^{-1})	V_D (v)	V_B (v)	η (%)	$-G_p$ ($\times 10^6 \text{Sm}^2$)	B_p ($\times 10^6 \text{S}^{-2}$)	f_p (GHz)	P_{out} (w)	$-Q_p$
Ka	3.59	532	945	17.9	1.75	2.13	38	1.56	1.21
V	3.7	387	693	17.7	2.27	6.69	55	1.09	2.94
W	3.91	152	348	13.9	5.53	27.4	87	0.66	4.9

The computed electric field profiles for the designed diode are shown in fig.2.It can be seen that the value of the peak electric field E_m increases with increasing the operating frequency as the width of the depletion layer decreases at high operating frequency. It can also be seen that the ratio of drift voltage (V_D) to the breakdown voltage (V_B) is highest for Ka-band diodes and then decreases for V-band and w-band diodes. More value of this ratio will be the more localized Avalanche zone which in turns provides high efficiency. From table3.it can be seen that conversion efficiency is higher (17.9%) for Ka band diodes than that of V band (17.7%) and w band (13.9%) respectively.

The high frequency simulation program has been used to obtain the admittance characteristics (Figure 3a, 3b and 3c) and negative resistivity profiles (4a, 4b and 4c) of the designed diodes. The integrated mm-wave properties such as diode negative conductance, susceptance, RF power and quality factor can be obtained from the admittance characteristic of the SDR diodes. Figure 3a, 3b and 3c show the variation of the diode negative conductance (-G) and susceptance (B) with frequencies for various considered frequency bands. The peak operating frequencies for Ka, V and W bands are found as 38 GHz, 55GHz and 87 GHz respectively. Though the negative conductance(- G_p) value is highest for the W band diode in comparison to the other two band diodes, the RF power contributed is of highest value for the Ka band diode (Table 3).The reason is explained as the RF power contributed by the IMPATT diode depends not only on the negative conductance (- G_p) but also on the RF voltage (V_{RF}) swing which in turn depends on breakdown voltage (approximately, $V_{RF} = V_B/5$) of the diode which is obtained highest for Ka band diode. Results of table 3 also shows that Ka band diode perform

better than other two band diodes in terms of quality factor (Q_p). To study the microscopic properties of the diodes, the authors have computed the spatial distribution of negative resistivity $[R(x)]$ in the depletion layer of the device, which would give an insight into the depletion region that contributes RF power. The obtained $R(x)$ profiles at respective optimum frequencies (f_p) are shown in figure 4a, 4b and 4c respectively. The computed $R(x)$ profiles in each case have one negative resistivity peak (R_{max}) in the middle of the drift layers. Again from the resistivity plot it can be seen that the resistivity peak shifts away from the junction as operating frequency increases. Which shows very good resembles with the earlier published work [Mukherjee et. al. 2005]. Moreover it is quite obvious that the contribution of negative resistivity is more from the drift region than that of the Avalanche region. This in turn indicates that drift zone contributes more mm-wave power than the avalanche zone. The results which are obtained in the present analysis shows very much similarity with earlier work done GaN (Wz) at D band [Panda et. al. 2001]. The present small signal analysis thus gives useful and interesting results regarding the role of GaN (Wz) in the generation of mm-wave frequencies.

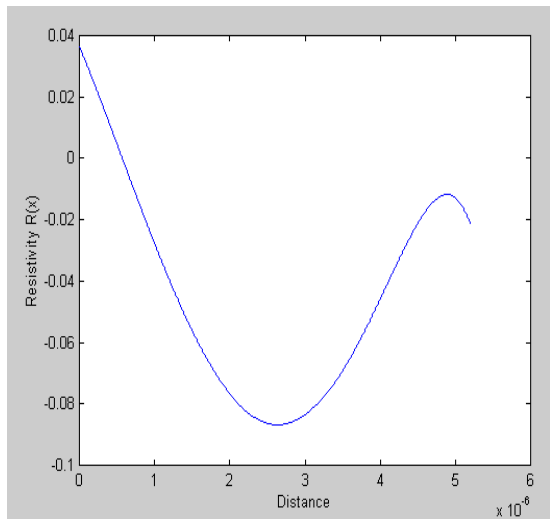
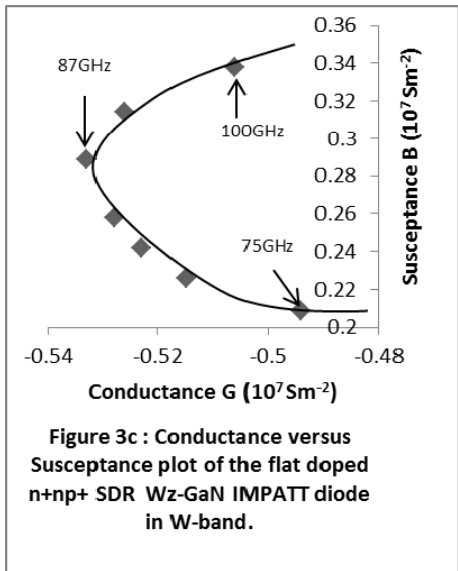
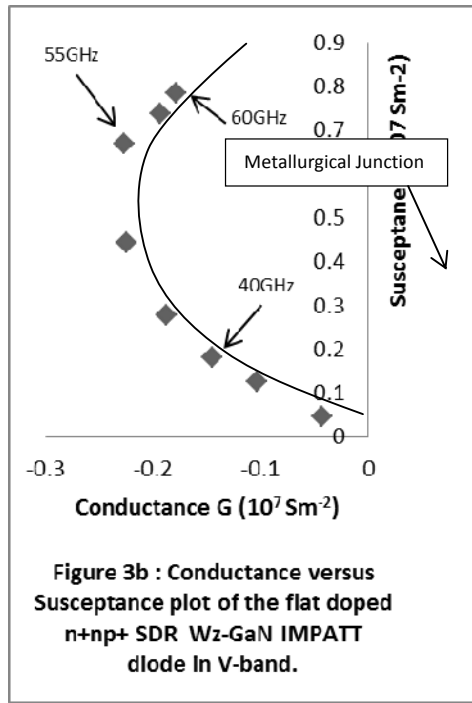
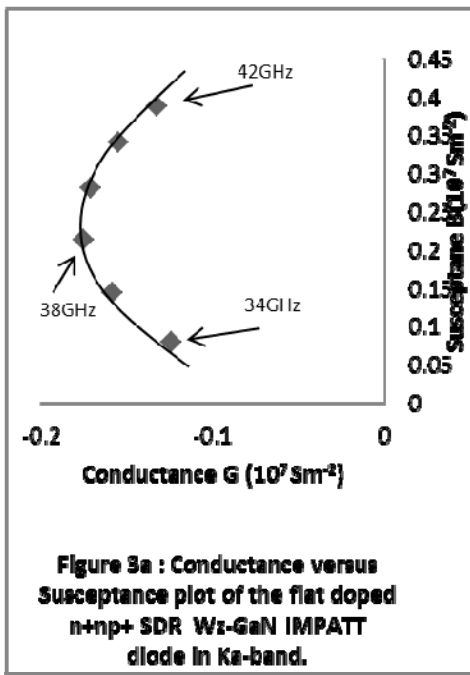


Figure 4(a)

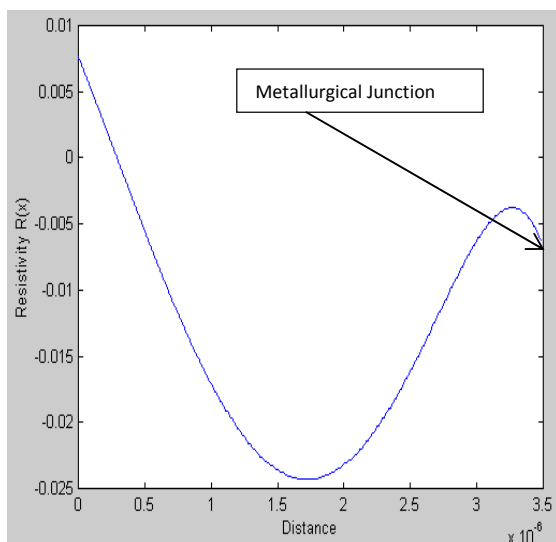


Figure 4(b):

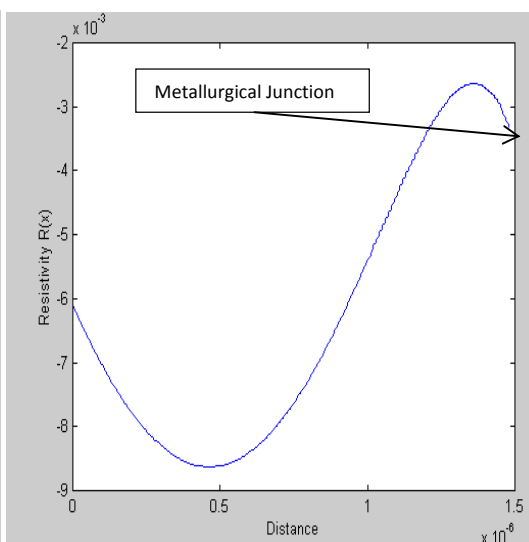


Figure 4(c):

Figure 4: Negative resistivity $[R(x)]$ profiles of flat doped GaN (Wz) based IMPATT diode observed in different frequency bands. (a) Plot of negative resistivity profile in Ka-band, (b) Plot of negative resistivity profile in V-band and (c) Plot of negative resistivity profile in W-band

4. Conclusions:

The simulation result provides a clear insight into the contributions of depletion layer in the generation of mm-wave power at different mm wave frequency bands for GaN based IMPATT. The analysis of this paper may be considered to be extremely helpful for the practical realization of GaN (Wz) based SDR IMPATT diodes at Ka-band and D-band for many civilian and military applications.

References:

- [1] Trew R J, (2005): "High frequency solid state electronic devices", Journal of IEEE Trans. Electron Devices vol.52, p.638.
- [2] Okumura H, (2006): "Present status and future prospect of wide gap semiconductor high-power devices", Japan. Journal of Appl. Phys., vol.45, p.7565
- [3] Inoki C K, Kaun T S, Lee C D., Sagar A, Feenstra R M, Koleske D D., Dfaz D Z., Bohn P W, and Adesida I, (2003) "Growth of GaN on porous SiC and GaN substrates", J.Electron. Materials, vol. 32, p.855.
- [4] Panda A K, Pavlidis D and Alekseev E, (2001): "DC and high frequency characteristics of GaN based IMPATTs", Journal of IEEE Trans. on Eletron Devices, vol.48, p.820.
- [5] Eisele H and Haddad G I, (1997): Active microwave devices, Microwave Semiconductor Device Physics, New York, p.343.
- [6] Electronic Archive. New semiconductor materials: characteristics and properties <http://www.ioffe.ru/SVA/NSM/Semicond/GaN>
- [7] Mukherjee M, Mazumder N, Roy S K and Goswami, P.K, (2007): "GaN IMPATT Diode : a photo sensitive high power terahertz source", Journal of Semiconductor. Science & Technology. vol.22, pp.1258-1267.
- [8] Kunihiro K, Kasahara K, Takahashi Y and Ohno Y, (1999): "Experimental evaluation of impact ionization coefficients in GaN", Journal of IEEE Electron Device Lett. Vol.20, p.608.
- [9] Sze, S. M,(1991): Physics of Semiconductor Devices, second ed., Wiley Eastern Limited.
- [10] Gummel H.K and Blue J.L., (1967): "Small Signal Theory of Avalanche Noise in IMPATT diodes", Journal of IEEE Trans. on Eletron Devices, vol.14, p.569.
- [11] Mukherjee M, and Roy, S. K. (2010): "Wide band gap III-IV nitride based avalanche transit time diode in terahertz regime: studies on the effects on punch through on high frequency characteristics and series resistance of the device", Journal of Applied Physics, vol.10, pp.646-651.
- [12] Mazumder, N and Roy, S. K. (1997): "Studies on pulsed mm-wave low-high-low Si IMPATT diodes at high current density and dependence on structural parameters", Journal of Semiconductor Science & Technology, vol.12, p. 623.
- [13] Mazumder N, Banerjee, J.P. and Roy S K (1989): "Variation of high frequency negative resistance of silicon n+pp+ and GaAs p+nn+ IMPATT diodes with enhancement of reverse saturation current ", Journal of Phys. Status Solidi A, vol.116, p.415.
- [14] Mukherjee M, Mazumder N and Roy S.K.,(2008): "Photo-sensitivity analysis of GaN and SiC terahertz IMPATT oscillator : comparison on theoretical reliability and study on experimental feasibility" Journal of IEEE Trans. on Device Mater Reliab., vol.8, pp. 608- 620.